J Sci Comput (2016) 68:848–863
DOI 10.1007/s10915-015-0161-x

An Adaptive P_1 Finite Element Method for Two-Dimensional Transverse Magnetic Time Harmonic Maxwell's Equations with General Material Properties and General Boundary Conditions

S. C. Brenner[1] · J. Gedicke[2] · L.-Y. Sung[1]

Received: 30 May 2015 / Revised: 6 December 2015 / Accepted: 29 December 2015 /
Published online: 1 February 2016

Abstract We present an adaptive P_1 finite element method for two-dimensional transverse magnetic time harmonic Maxwell's equations with general material properties and general boundary conditions. It is based on reducing the boundary value problems for Maxwell's equations to standard second order scalar elliptic problems through the Hodge decomposition. We allow inhomogeneous and anisotropic electric permittivity, sign changing magnetic permeability, and both the perfectly conducting boundary condition and the impedance boundary condition. The optimal convergence of the adaptive finite element method is demonstrated by numerical experiments. We also present results for a semiconductor simulation, a cloaking simulation and a flat lens simulation that illustrate the robustness of the method.

Keywords Adaptivity · Error estimators · Finite element method · Hodge decomposition · Maxwell's equations · Impedance boundary condition · Metamaterials · Cloaking · Flat lens

1 Introduction

A new approach to two-dimensional time-harmonic Maxwell's equations with the perfectly conducting boundary condition was introduced in [3], where the problem was reduced to

The work of the first and third authors was supported in part by the National Science Foundation under Grant No. DMS-13-19172. The work of the second author was supported by a fellowship within the Postdoc-Program of the German Academic Exchange Service (DAAD).

✉ S. C. Brenner
brenner@math.lsu.edu

J. Gedicke
joscha.gedicke@iwr.uni-heidelberg.de

[1] Department of Mathematics, Center for Computation and Technology, Louisiana State University, Baton Rouge, LA 70803, USA

[2] Interdisziplinäres Zentrum für Wissenschaftliches Rechnen (IWR), Universität Heidelberg, Im Neuenheimer Feld 368, 69120 Heidelberg, Germany

standard second order scalar elliptic boundary value problems through the Hodge decomposition. This approach makes it possible to apply many standard numerical techniques to computational electromagnetics. A P_1 finite element method based on this approach was analyzed in [3]. Adaptive versions and multigrid algorithms for the P_1 finite element method were subsequently developed in [4,6].

In a recent paper [5], the Hodge decomposition approach was extended to transverse magnetic problems that involve general materials and the impedance boundary condition. The goal of this paper is to extend the adaptive methods in [4] to the general problem for time-harmonic Maxwell's equations treated in [5], whose setting is recalled below.

We take the material domain $\Omega \subset \mathbb{R}^2$ to be a bounded polygon whose boundary consists of two disjoint closed subsets Γ_{pc} (where the perfectly conducting boundary condition is posed) and Γ_{imp} (where the impedance boundary condition is posed). We denote the magnetic permeability by μ, the electric permittivity by ϵ, the impedance on Γ_{imp} by $1/\lambda$, the electric current density by $\boldsymbol{f}$, and the magnetic field density imposed on Γ_{imp} by g.

We assume that $\boldsymbol{f} \in [L_2(\Omega)]^2$ (the space of complex L_2 vector fields on Ω), $g \in L_2(\Gamma_{\text{imp}})$ (the space of complex L_2 functions on Γ_{imp}), λ is a smooth strictly positive function defined on Γ_{imp}, μ and $1/\mu$ are real-valued functions in $L_\infty(\Omega)$, and ϵ is a smooth real symmetric positive definite 2×2 tensor field defined on $\bar{\Omega}$.

Remark 1 Note that the magnetic permeability μ is allowed to change sign in our setting, and the electric permittivity can be inhomogeneous and anisotropic. We will also allow ϵ to change sign in the numerical experiment for a flat lens. Thus the results in this paper are also relevant for electromagnetic problems involving metamaterials [12,19].

The model transverse magnetic problem is to find $\boldsymbol{u} \in \mathbb{E}$ such that

$$(\mu^{-1}\nabla \times \boldsymbol{u}, \nabla \times \boldsymbol{v}) - k^2(\epsilon \boldsymbol{u}, \boldsymbol{v}) - ik\langle \lambda \boldsymbol{n} \times \boldsymbol{u}, \boldsymbol{n} \times \boldsymbol{v}\rangle_{\Gamma_{\text{imp}}} = (\boldsymbol{f}, \boldsymbol{v}) + \langle g, \boldsymbol{n} \times \boldsymbol{v}\rangle_{\Gamma_{\text{imp}}} \quad (1)$$

for all $\boldsymbol{v} \in \mathbb{E}$.

Here $i = \sqrt{-1}$, $k > 0$ is the frequency, $(\cdot, \cdot)$ (resp. $\langle \cdot, \cdot \rangle_{\Gamma_{\text{imp}}}$) denotes the inner product of the complex function space $[L_2(\Omega)]^2$ (resp. $L_2(\Gamma_{\text{imp}})$),

$$\mathbb{E} = H_{\text{imp}}(\text{curl}; \Omega; \Gamma_{\text{imp}}) \cap H_0(\text{curl}; \Omega; \Gamma_{\text{pc}}) \cap H(\text{div}^0; \Omega; \epsilon),$$

and the spaces $H_{\text{imp}}(\text{curl}; \Omega; \Gamma_{\text{imp}})$, $H_0(\text{curl}; \Omega; \Gamma_{\text{pc}})$ and $H(\text{div}^0; \Omega; \epsilon)$ are defined as follows:

$$\begin{aligned}
H(\text{curl}; \Omega) &= \left\{ \boldsymbol{v} = \begin{bmatrix} v_1 \\ v_2 \end{bmatrix} \in [L_2(\Omega)]^2 : \nabla \times \boldsymbol{v} = \partial v_2/\partial x_1 - \partial v_1/\partial x_2 \in L_2(\Omega) \right\}, \\
H_{\text{imp}}(\text{curl}; \Omega; \Gamma_{\text{imp}}) &= \left\{ \boldsymbol{v} \in H(\text{curl}; \Omega) : \boldsymbol{n} \times \boldsymbol{v}\big|_{\Gamma_{\text{imp}}} \in L_2(\Gamma_{\text{imp}}) \right\}, \\
H_0(\text{curl}; \Omega; \Gamma_{\text{pc}}) &= \left\{ \boldsymbol{v} \in H(\text{curl}; \Omega) : \boldsymbol{n} \times \boldsymbol{v}\big|_{\Gamma_{\text{pc}}} = 0 \right\}, \\
H(\text{div}^0; \Omega) &= \left\{ \boldsymbol{v} = \begin{bmatrix} v_1 \\ v_2 \end{bmatrix} \in [L_2(\Omega)]^2 : 0 = \nabla \cdot \boldsymbol{v} = \partial v_1/\partial x_1 + \partial v_2/\partial x_2 \right\}, \\
H(\text{div}^0; \Omega; \epsilon) &= \left\{ \boldsymbol{v} \in [L_2(\Omega)]^2 : \epsilon \boldsymbol{v} \in H(\text{div}^0; \Omega) \right\},
\end{aligned}$$

where $\boldsymbol{n} = (n_1, n_2)^t$ is the outward pointing unit normal along $\partial\Omega$ and $\boldsymbol{n} \times \boldsymbol{v} = n_1 v_2 - n_2 v_1$ is the tangential component of $\boldsymbol{v}$.

Note that (1) is well-posed for k outside a (possibly empty) discrete subset of $\mathbb{R}_+$ [5,11].

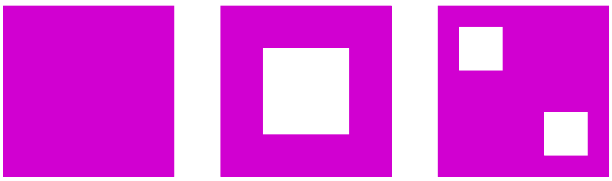

Fig. 1 Betti numbers for Ω

Remark 2 In the case where Γ_{imp} is the outer boundary of Ω and Γ_{pc} is the inner boundary of Ω (cf. Fig. 1), problem (1) can be used to model a truncated scattering problem where Γ_{pc} is the boundary of the scatterer(s) and the impedance boundary condition acts as an absorbing boundary condition [11,18].

The rest of the paper is organized as follows. We first recall the Hodge decomposition approach to (1) in Sect. 2. We then develop an adaptive P_1 finite element method in Sect. 3. Numerical results are presented in Sect. 4 and we end with some concluding remarks in Sect. 5.

Throughout this paper we use the notation $x \lesssim y$ to represent the inequality $x \leq C_1 y$ and the notation $x \approx y$ to represent the inequalities $C_2 y \leq x \leq C_1 y$, with constants $C_1, C_2 > 0$ that do not depend on the mesh size but may depend on ϵ, μ, and k.

2 The Hodge Decomposition Approach

Let the nonnegative integer m be the Betti number of Ω (cf. Fig. 1). In the Hodge decomposition approach for (1), we write the electric field $\boldsymbol{u}$ as

$$\boldsymbol{u} = \epsilon^{-1}\nabla \times \phi + \sum_{j=1}^{m} c_j \nabla \varphi_j, \tag{2}$$

where $\phi \in H^1(\Omega)$ satisfies $(\phi, 1) = 0$ and the functions $\varphi_1, \ldots, \varphi_m$ are defined as follows.

Let the outer boundary of Ω be denoted by Γ_0 and the m components of the inner boundary be denoted by $\Gamma_1, \ldots, \Gamma_m$. Then the functions $\varphi_j \in H^1(\Omega)$ for $1 \leq j \leq m$ are determined by the scalar problems

$$(\epsilon \nabla \varphi_j, \nabla v) = 0 \quad \forall\, v \in H_0^1(\Omega), \tag{3a}$$

$$\varphi_j|_{\Gamma_0} = 0 \quad \text{and} \quad \varphi_j|_{\Gamma_l} = \delta_{jl} \quad \text{for } 1 \leq l \leq m, \tag{3b}$$

where $\delta_{jl} = 1$ if $j = l$ and $\delta_{jl} = 0$ if $j \neq l$.

It was shown in [5, Section 2] that there exists a discrete subset S_+ of $\mathbb{R}_+$ such that the model problem (1) is uniquely solvable for $k \in \mathbb{R}_+ \backslash S_+$, in which case the function ϕ in (2) is determined by

$$(\nabla \times \phi, \epsilon^{-1}\nabla \times \psi) = \frac{i}{k}\langle (\xi - g)/\lambda, \psi \rangle_{\Gamma_{\text{imp}}} + (\mu \xi, \psi) \qquad \forall\, \psi \in H^1(\Omega) \tag{4}$$

together with the constraint $(\phi, 1) = 0$, and the function $\xi = \mu^{-1}\nabla \times \boldsymbol{u} \in H^1(\Omega)$ (which is the magnetic field multiplied by $-ik$) is determined by

$$\begin{aligned}&(\nabla \times \xi, \epsilon^{-1}\nabla \times \psi) - k^2(\mu\xi, \psi) - ik\langle \xi/\lambda, \psi\rangle_{\Gamma_{\text{imp}}} \\ &\quad = (\boldsymbol{f}, \epsilon^{-1}\nabla \times \psi) - ik\langle g/\lambda, \psi\rangle_{\Gamma_{\text{imp}}} \qquad \forall\, \psi \in H^1(\Omega). \end{aligned} \tag{5}$$

Remark 3 The discrete subset S_+ (possibly empty) is determined by the well-posedness of the Fredholm problem (5). For $k \in \mathbb{R}_+ \backslash S_+$, the solution of (5) satisfies

$$(\mu\xi, 1) = \frac{i}{k}\langle (g - \xi)/\lambda, 1\rangle_{\Gamma_{\text{imp}}}, \tag{6}$$

which then implies that the singular Neumann problem (4) is solvable.

In the case where $m \geq 1$ the coefficients c_j in (2) are determined by the symmetric positive definite system

$$\sum_{j=1}^{m}(\epsilon\nabla\varphi_j, \nabla\varphi_l)c_j = -\frac{1}{k^2}(\boldsymbol{f}, \nabla\varphi_l) \qquad \text{for } 1 \leq l \leq m. \tag{7}$$

From now on we assume that $k \in \mathbb{R}_+ \backslash S_+$. We can then solve (1) numerically by the following P_1 finite element method.

Let $\mathcal{T}_\ell$ be a regular triangulation of Ω with mesh size $h_\ell = \max_{T\in\mathcal{T}_\ell} h_T$, where $h_T = \operatorname{diam} T$, and let $V_\ell \subset H^1(\Omega)$ be the P_1 finite element space associated with $\mathcal{T}_\ell$. The space $V_\ell \cap H_0^1(\Omega)$ is denoted by $\mathring{V}_\ell$.

First we find an approximate solution of (5) by computing $\xi_\ell \in V_\ell$ such that

$$\begin{aligned}&(\nabla \times \xi_\ell, \epsilon^{-1}\nabla \times \psi_\ell) - k^2(\mu\xi_\ell, \psi_\ell) - ik\langle \xi_\ell/\lambda, \psi_\ell\rangle_{\Gamma_{\text{imp}}} \\ &\quad = (\boldsymbol{f}, \epsilon^{-1}\nabla \times \psi_\ell) - ik\langle g/\lambda, \psi_\ell\rangle_{\Gamma_{\text{imp}}} \qquad \forall\, \psi_\ell \in V_\ell. \end{aligned} \tag{8}$$

Then we find an approximate solution of (4) by replacing ξ with ξ_ℓ and computing $\phi_\ell \in V_\ell$ such that $(\phi_\ell, 1) = 0$ and

$$(\nabla \times \phi_\ell, \epsilon^{-1}\nabla \times \psi_\ell) = \frac{i}{k}\langle (\xi_\ell - g)/\lambda, \psi_\ell\rangle_{\Gamma_{\text{imp}}} + (\mu\xi_\ell, \psi_\ell) \qquad \forall\, \psi \in V_\ell. \tag{9}$$

If Ω is not simply connected ($m \geq 1$), we find approximate solutions of (3a, 3b) by computing $\varphi_{1,\ell}, \ldots, \varphi_{m,\ell} \in V_\ell$ such that

$$(\epsilon\nabla\varphi_{j,\ell}, \nabla v_\ell) = 0 \qquad \forall\, v_\ell \in \mathring{V}_\ell, \tag{10a}$$

$$\varphi_{j,\ell}|_{\Gamma_0} = 0 \quad \text{and} \quad \varphi_{j,\ell}|_{\Gamma_l} = \delta_{jl} \quad \text{for } 1 \leq l \leq m, \tag{10b}$$

and then we find an approximate solution of (7) by replacing φ_j with $\varphi_{j,\ell}$ and solving

$$\sum_{j=1}^{m}(\epsilon\nabla\varphi_{j,\ell}, \nabla\varphi_{l,\ell})c_{j,\ell} = -\frac{1}{k^2}(\boldsymbol{f}, \nabla\varphi_{l,\ell}) \quad \text{for } 1 \leq l \leq m. \tag{11}$$

The approximate solution of (1) is given by

$$\boldsymbol{u}_\ell = \epsilon^{-1}\nabla \times \phi_\ell + \sum_{j=1}^{m} c_{j,\ell}\nabla\varphi_{j,\ell}. \tag{12}$$

The a priori error analysis of this P_1 finite element method can be found in [5, Section 3].

Remark 4 The scalar functions ϕ and ξ become vector fields for the Hodge decomposition in three dimensions and hence (1) will not be reduced to scalar problems.

3 An Adaptive P_1 Finite Element Method

We will use the following notation in the *a posteriori* error analysis. Let $\mathcal{E}_\ell$ (resp. $\mathcal{E}_\ell^i$) denote the set of edges (resp. interior edges) and h_e denote the length of $e \in \mathcal{E}_\ell$. For $e \in \mathcal{E}_\ell^i$, let $T_\pm \in \mathcal{T}_\ell$ be the two neighboring triangles that share the edge e and $\boldsymbol{n}_\pm$ be the unit normal of E pointing towards the outside of $T_\pm$. The normal jump of a piecewise smooth vector field $\boldsymbol{v}$ across e is defined by $[\![\boldsymbol{n}_e \cdot \boldsymbol{v}]\!] = \boldsymbol{n}_+ \cdot \boldsymbol{v}_+ + \boldsymbol{n}_- \cdot \boldsymbol{v}_-$ and the tangential jump across e is defined by $[\![\boldsymbol{n}_e \times \boldsymbol{v}]\!] = \boldsymbol{n}_+ \times \boldsymbol{v}_+ + \boldsymbol{n}_- \times \boldsymbol{v}_-$, where $\boldsymbol{v}_\pm = \boldsymbol{v}\big|_{T_\pm}$.

Using (2), (12) and the triangle inequality, it is straightforward (cf. [4, Lemma 1]) to show that

$$\|\boldsymbol{u} - \boldsymbol{u}_\ell\|_{L_2(\Omega;\epsilon)} \lesssim \|\epsilon^{-1}\nabla \times (\phi - \phi_\ell)\|_{L_2(\Omega;\epsilon)} + \sum_{j=1}^{m} \|\nabla\varphi_j - \nabla\varphi_{j,\ell}\|_{L_2(\Omega;\epsilon)}, \tag{13}$$

where $\|\boldsymbol{v}\|_{L_2(\Omega;\epsilon)} = \left(\int_\Omega (\epsilon\boldsymbol{v}) \cdot \bar{\boldsymbol{v}}\, dx\right)^{\frac{1}{2}}$.

The following estimate for the second term on the right-hand side of (13) is also standard (cf., for example, [10, Section 3.2.1] and the references therein).

Lemma 1 *Let $\varphi_{j,\ell} \in V_\ell$, $j = 1, \ldots, m$, be the solutions of* (10a, 10b)*. We have*

$$\|\nabla(\varphi_j - \varphi_{j,\ell})\|^2_{L_2(\Omega;\epsilon)} \lesssim \sum_{T\in\mathcal{T}_\ell} h_T^2 \|\nabla \cdot (\epsilon\nabla\varphi_{j,\ell})\|^2_{L_2(T)} + \sum_{e\in\mathcal{E}_\ell^i} h_e \|[\![\boldsymbol{n}_e \cdot \epsilon\nabla\varphi_{j,\ell}]\!]\|^2_{L_2(E)}.$$

The next lemma provides an estimate for the first term on the right-hand side of (13).

Lemma 2 *Let ϕ_ℓ be the solution of* (9)*. We have*

$$\begin{aligned}
\|\epsilon^{-1}\nabla \times (\phi - \phi_\ell)\|^2_{L_2(\Omega;\epsilon)} &\lesssim \sum_{T\in\mathcal{T}_\ell} h_T^2 \|\mu\xi_\ell - \nabla \times (\epsilon^{-1}\nabla \times \phi_\ell)\|^2_{L_2(T)} \\
&+ \sum_{e\in\mathcal{E}_\ell^i} h_e \|[\![\boldsymbol{n}_e \times (\epsilon^{-1}\nabla \times \phi_\ell)]\!]\|^2_{L_2(e)} + \sum_{e\subset\Gamma_{\mathrm{pc}}} h_e \|\boldsymbol{n} \times (\epsilon^{-1}\nabla \times \phi_\ell)\|^2_{L_2(e)} \\
&+ \sum_{E\subset\Gamma_{\mathrm{imp}}} h_e \|\boldsymbol{n} \times (\epsilon^{-1}\nabla \times \phi_\ell) + \frac{i}{k}(\xi_\ell - g)/\lambda\|^2_{L_2(e)} \\
&+ \|\xi - \xi_\ell\|^2_{L_2(\Omega)} + \|\xi - \xi_\ell\|^2_{L_2(\Gamma_{\mathrm{imp}})},
\end{aligned}$$

where ξ_ℓ is the solution of (8)*.*

Proof It follows from (4) that

$$\begin{aligned}
&\|\epsilon^{-1}\nabla \times (\phi - \phi_\ell)\|^2_{L_2(\Omega;\epsilon)} \\
&\quad = -(\epsilon^{-1}\nabla \times \phi_\ell, \nabla \times (\phi - \phi_\ell)) + \frac{i}{k}\langle(\xi - g)/\lambda, \phi - \phi_\ell\rangle_{\Gamma_{\mathrm{imp}}} + (\mu\xi, \phi - \phi_\ell) \\
&\quad = \mathrm{Res}_\ell(\phi - \phi_\ell) + \frac{i}{k}\langle(\xi - \xi_\ell)/\lambda, \phi - \phi_\ell\rangle_{\Gamma_{\mathrm{imp}}} + (\mu(\xi - \xi_\ell), \phi - \phi_\ell),
\end{aligned}$$

where

$$\mathrm{Res}_\ell(\psi) = \frac{i}{k}\langle(\xi_\ell - g)/\lambda, \psi\rangle_{\Gamma_{\mathrm{imp}}} + (\mu\xi_\ell, \psi) - (\epsilon^{-1}\nabla \times \phi_\ell, \nabla \times \psi) \qquad \forall\, \psi \in H^1(\Omega).$$

Hence we have

$$\|\epsilon^{-1}\nabla\times(\phi-\phi_\ell)\|^2_{L_2(\Omega;\epsilon)} \le \|\mathrm{Res}_\ell\|_*\|\nabla\times(\phi-\phi_\ell)\|_{L_2(\Omega)} + \|\mu(\xi-\xi_\ell)\|_{L_2(\Omega)}\|\phi-\phi_\ell\|_{L_2(\Omega)} + \frac{1}{k}\|(\xi-\xi_\ell)/\lambda\|_{L_2(\Gamma_{\mathrm{imp}})}\|\phi-\phi_\ell\|_{L_2(\Gamma_{\mathrm{imp}})}, \quad (14)$$

where $\|\mathrm{Res}_\ell\|_* = \sup_{\psi\in H^1(\Omega)}\mathrm{Res}_\ell(\psi)/\|\psi\|_{H^1(\Omega)}$.

Since $(\phi-\phi_\ell, 1) = 0$, we can apply a Poincaré-Friedrichs inequality and a trace inequality to deduce from (14) that

$$\|\epsilon^{-1}\nabla\times(\phi-\phi_\ell)\|_{L_2(\Omega;\epsilon)} \lesssim \|\mathrm{Res}_\ell\|_* + \|\mu(\xi-\xi_\ell)\|_{L_2(\Omega)} + \frac{1}{k}\|(\xi-\xi_\ell)/\lambda\|_{L_2(\Gamma_{\mathrm{imp}})},$$

and it only remains to estimate $\|\mathrm{Res}_\ell\|_*$.

For any $\psi_\ell \in V_\ell$, we have $\mathrm{Res}_\ell(\psi_\ell) = 0$ because of (9). Integration by parts then leads to

$$\begin{aligned}\mathrm{Res}_\ell(\psi) &= \mathrm{Res}_\ell(\psi-\psi_\ell)\\ &= \sum_{T\in\mathcal{T}_\ell}\int_T h_T(\mu\xi_\ell - \nabla\times(\epsilon^{-1}\nabla\times\phi_\ell))h_T^{-1}\overline{(\psi-\psi_\ell)}\,dx\\ &\quad+\sum_{e\in\mathcal{E}_\ell^i}\int_e h_e^{1/2}[\![\boldsymbol{n}_e\times(\epsilon^{-1}\nabla\times\phi_\ell)]\!]h_e^{-1/2}\overline{(\psi-\psi_\ell)}\,ds\\ &\quad+\sum_{e\subset\Gamma_{\mathrm{pc}}}\int_e h_e^{1/2}\left(\boldsymbol{n}\times(\epsilon^{-1}\nabla\times\phi_\ell)\right)h_e^{-1/2}\overline{(\psi-\psi_\ell)}\,ds\\ &\quad+\sum_{e\subset\Gamma_{\mathrm{imp}}}\int_e h_e^{1/2}\left(\boldsymbol{n}\times(\epsilon^{-1}\nabla\times\phi_\ell)+\frac{i}{k}(\xi_\ell-g)/\lambda\right)h_e^{-1/2}\overline{(\psi-\psi_\ell)}\,ds.\end{aligned}$$

The estimate for $\|\mathrm{Res}_\ell\|_*$ (and the proof of the lemma) is completed by the Cauchy-Schwarz inequality after choosing $\psi_\ell \in V_\ell$ such that (cf. [17])

$$\sum_{T\in\mathcal{T}_\ell}\|h_T^{-1}(\psi-\psi_\ell)\|^2_{L_2(T)} + \sum_{e\in\mathcal{E}_\ell}\|h_e^{-1/2}(\psi-\psi_\ell)\|^2_{L_2(e)} \lesssim \|\nabla\psi\|^2_{L_2(\Omega)}.$$

□

Remark 5 If $\boldsymbol{f} \in [H^1(\Omega)]^2$ and $g \in H^{\frac{1}{2}}(E)$ for all the edges E of Ω that belong to Γ_{imp} (which is the case for all the numerical experiments in Sect. 4), then $\|\xi-\xi_\ell\|_{L_2(\Omega)}$ and $\|\xi-\xi_\ell\|_{L_2(\Gamma_{\mathrm{imp}})}$ are of higher order compared with $\|\boldsymbol{u}-\boldsymbol{u}_\ell\|_{L_2(\Omega)}$ (cf. [3, Remark 4.4] and [5, Theorem 3.8 and Corollary 3.3]).

Based on (13), Lemma 1, Lemma 2 and Remark 5, we define the local error indicator $\eta_\ell(T)$ by

$$\eta_\ell^2(T) = \sum_{j=1}^{m} h_T^2 \|\nabla \cdot (\epsilon \nabla \varphi_{j,\ell})\|_{L_2(T)}^2 + \sum_{j=1}^{m} \sum_{e \subset \partial T, e \in \mathcal{E}_\ell^i} h_e \|[\![\boldsymbol{n}_e \cdot \epsilon \nabla \varphi_{j,\ell}]\!]\|_{L_2(e)}^2$$
$$+ h_T^2 \|\mu \xi_\ell - \nabla \times (\epsilon^{-1} \nabla \times \boldsymbol{\phi}_\ell)\|_{L_2(T)}^2 + \sum_{e \subset \partial T, e \in \mathcal{E}_\ell^i} h_e \|[\![\boldsymbol{n}_e \times (\epsilon^{-1} \nabla \times \boldsymbol{\phi}_\ell)]\!]\|_{L_2(e)}^2$$
$$+ \sum_{e \subset \partial T, e \subset \Gamma_{\mathrm{pc}}} h_e \|\boldsymbol{n} \times (\epsilon^{-1} \nabla \times \boldsymbol{\phi}_\ell)\|_{L_2(e)}^2$$
$$+ \sum_{e \subset \partial T, e \subset \Gamma_{\mathrm{imp}}} h_e \|\boldsymbol{n} \times (\epsilon^{-1} \nabla \times \boldsymbol{\phi}_\ell) + \frac{i}{k}(\xi_\ell - g)/\lambda\|_{L_2(e)}^2, \tag{15}$$

where the terms involving $\xi - \xi_\ell$ are ignored. The global error estimator η_ℓ then reads $\eta_\ell = \left(\sum_{T \in \mathcal{T}_\ell} \eta_\ell^2(T)\right)^{1/2}$.

Remark 6 Under the conditions in Remark 5, the estimator η_ℓ is reliable up to higher order terms. Its efficiency will be demonstrated by the numerical experiments in Sect. 4.

We can now use the adaptive loop

$$\text{Solve} \rightarrow \text{Estimate} \rightarrow \text{Mark} \rightarrow \text{Refine}$$

to generate a sequence of triangulations $\mathcal{T}_0, \mathcal{T}_1, \ldots$ with associated finite element spaces $V_0 \subsetneq V_1 \subsetneq \ldots \subset V$ and approximate solutions ξ_ℓ and $\boldsymbol{u}_\ell$ for $\ell \geq 0$.

- Solve
  The approximate solutions ξ_ℓ and $\boldsymbol{u}_\ell$ on the mesh $\mathcal{T}_\ell$ are computed by the procedure described in (8)–(12).
- Estimate
  The error $\|\boldsymbol{u} - \boldsymbol{u}_\ell\|_{L_2(\Omega;\epsilon)}$ is estimated by the *a posteriori* error estimator η_ℓ defined in (15).
- Mark
  Based on the local refinement indicator $\eta_\ell(T)$, the elements in $\mathcal{T}_\ell$ are marked for refinement using a bulk criterion [7] with parameter $0 < \theta < 1$. It results in a minimal set $\mathcal{M}_\ell \subset \mathcal{T}_\ell$ of marked triangles that satisfies
  $$\theta \sum_{T \in \mathcal{T}_\ell} \eta_\ell^2(T) \leq \sum_{T \in \mathcal{M}_\ell} \eta_\ell^2(T).$$
- Refine
  Once a triangle is marked for refinement, all of its edges are marked for refinement. In a closure algorithm additional edges are marked for refinement such that if an edge of a triangle is marked for refinement, then the reference edge of that triangle is marked as well. After the closure algorithm has been applied the triangles are refined by one of the *red-green-blue* refinement rules depicted in Fig. 2.

4 Numerical Experiments

In this section we present some numerical examples for the model problem (1) with inhomogeneous material parameters and sign changing μ. We also demonstrate the robustness of

our method with the numerical results of a semiconductor simulation, a cloaking simulation and a flat lens simulation (where ϵ also changes signs) that are not covered by the a priori analysis in [5] or the *a posteriori* analysis in Sect. 3. In all numerical experiments we take λ to be 1.

4.1 Inhomogeneous and Anisotropic Medium

The first example considers the square domain $\Omega = (-1, 1)^2$ with inhomogeneous material parameters [9]

$$\epsilon = \begin{pmatrix} 1+x^2 & xy \\ xy & 1+y^2 \end{pmatrix} \quad \text{and} \quad \mu = (1+x^2+y^2)^{-1}.$$

For $k = 1$, we chose the analytic solution

$$u = \left(y/(x^2+y^2+0.02), -x/(x^2+y^2+0.02)\right)^t,$$

and compute $\boldsymbol{f}$ accordingly. The impedance boundary condition on $\partial\Omega$ is given by the exact solution. Figure 3 shows that both uniform and adaptive refinement lead to optimal $\mathcal{O}(N_\ell^{-1/2})$ convergence for the error $\|\boldsymbol{u} - \boldsymbol{u}_\ell\|_{L_2(\Omega;\epsilon)}$, where N_ℓ is the dimension of V_ℓ. (Note that for uniform refinement $N_\ell^{-1/2} \approx h_\ell$.) The *a posteriori* error estimator η_ℓ is empirically shown to be reliable and efficient. We also observe that the errors $\|\xi - \xi_\ell\|_{L_2(\Omega)}$ and $\|\xi - \xi_\ell\|_{L_2(\partial\Omega)}$ (not shown) are of higher order for both uniform and adaptive mesh refinements.

4.2 L-Shaped Domain

The second example concerns the L-shaped domain $\Omega = (-1, 1)^2 \backslash [0, 1]^2$ with sign changing μ. Such parameters occur in the study of metamaterials. For this example we chose $\epsilon = 1$, $\mu = 1$ in quadrant III and $\mu = -1$ in quadrant II and IV. We chose the homogenous impedance boundary condition $g = 0$, the right-hand side $\boldsymbol{f}$ to be $(1, 1)^t$, and the frequency k to be 1. Since the exact solution is unknown, we compute the errors by using a reference solution which is computed on a uniform refinement of the finest (adaptive) mesh.

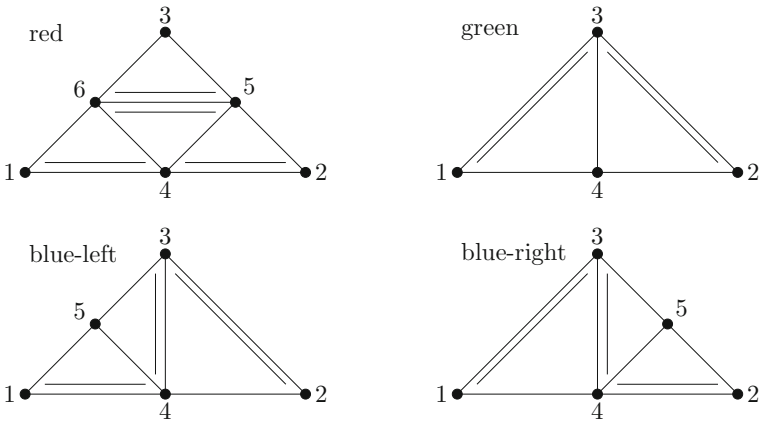

Fig. 2 Refinement rules: *sub-triangles* with corresponding *reference edges* depicted with a second edge

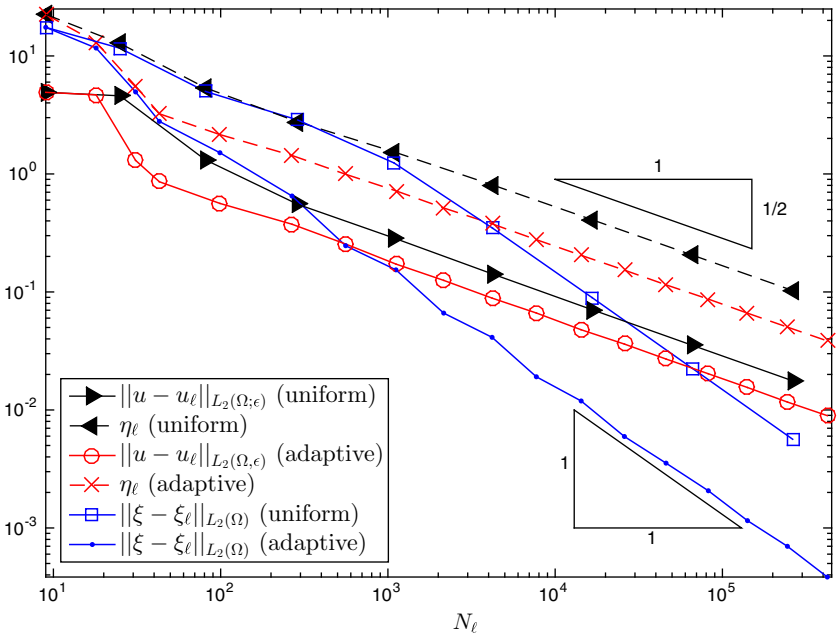

Fig. 3 Convergence history for the first example

The convergence history for the error $\|u-u_\ell\|_{L_2(\Omega)}$ is shown in Fig. 4. Since the solution has a singularity at the origin, uniform refinement leads to sub-optimal convergence while adaptive refinement recovers optimal convergence $\mathcal{O}(N_\ell^{-1/2})$. Note that the errors $\|\xi - \xi_\ell\|_{L_2(\Omega)}$ and $\|\xi - \xi_\ell\|_{L_2(\partial\Omega)}$ (not shown) are of higher order for both uniform and adaptive refinement.

4.3 Doubly Connected Domain

The third example involves the doubly connected domain $\Omega = (-1,1)^2\backslash[-1/2,1/2]$. We chose $\epsilon = 1$, $\mu = 1$, $k = 1$, the homogenous impedance boundary condition $g = 0$ on the outer boundary and the homogeneous perfectly conducting boundary condition $\boldsymbol{n}\times\boldsymbol{u} = 0$ on the inner part of the boundary. As right-hand side we chose $\boldsymbol{f} = (e^{x_1}, e^{x_2})^t$ so that the coefficient c in the Hodge decomposition for $\boldsymbol{u}$ is nonzero. Thus we have to solve three scalar equation for this example.

We approximate the unknown error as in the previous example and observe that uniform refinement leads to sub-optimal convergence rates as displayed in Fig. 5 for the error $\|\boldsymbol{u} - \boldsymbol{u}_\ell\|_{L_2(\Omega)}$. In contrast, adaptive refinement leads to optimal convergence $\mathcal{O}(N_\ell^{-1/2})$. Note that in both cases $\|\xi - \xi_\ell\|_{L_2(\Omega)}$ and $\|\xi - \xi_\ell\|_{L_2(\Gamma_{\text{imp}})}$ (not shown) are of higher order.

4.4 Semiconductor Simulation

In this example we demonstrate that the results in [3,5] can be extended to the case where ϵ is complex-valued. We consider a cavity problem where a conductor is wrapped inside a semiconductor. The domain Ω is the doubly connected domain $(-1,1)^2\backslash[-1/4,1/4]$. We take ϵ to be 1 (resp. $1+i/2$) outside (resp. inside) the square $[-1/2,1/2]$. We choose $\mu = 1$,

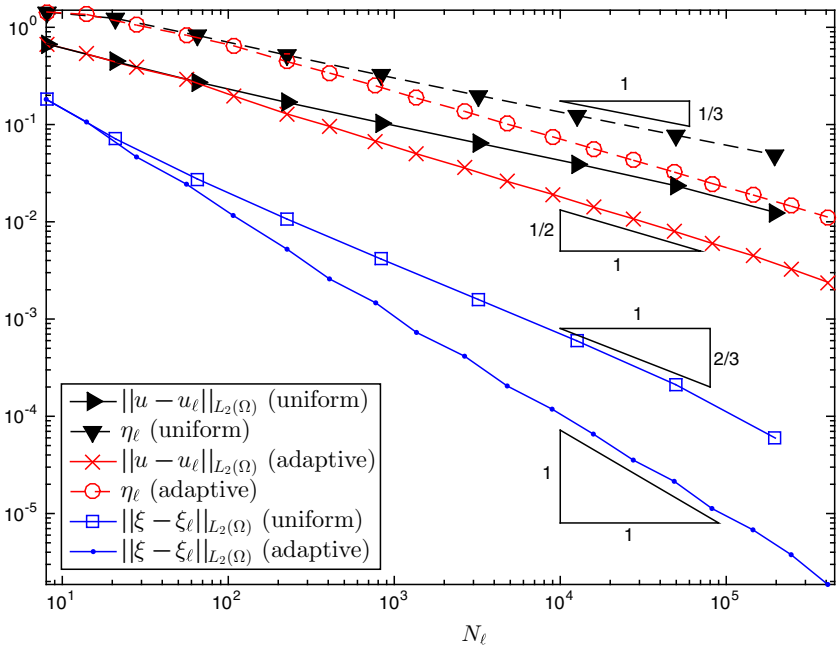

Fig. 4 Convergence history for the L-shaped domain

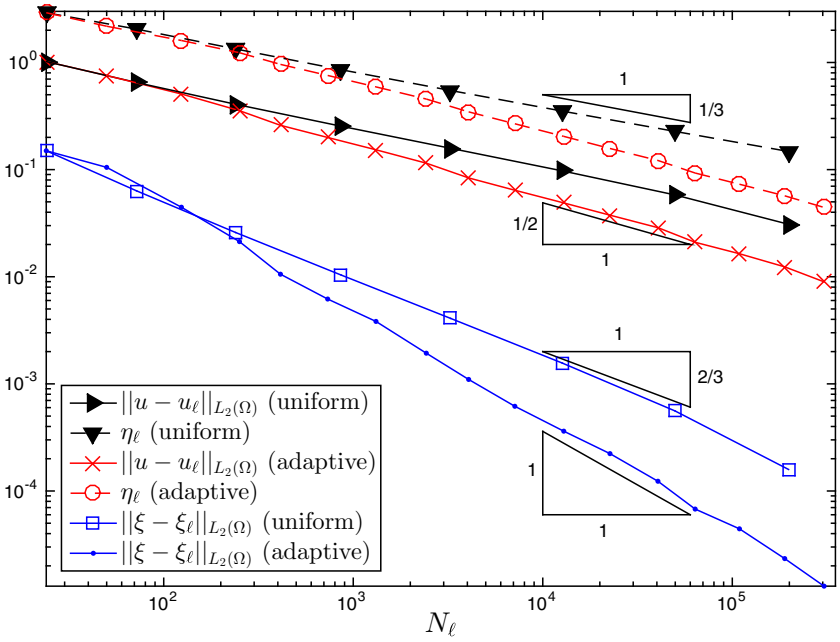

Fig. 5 Convergence history for the doubly connected domain

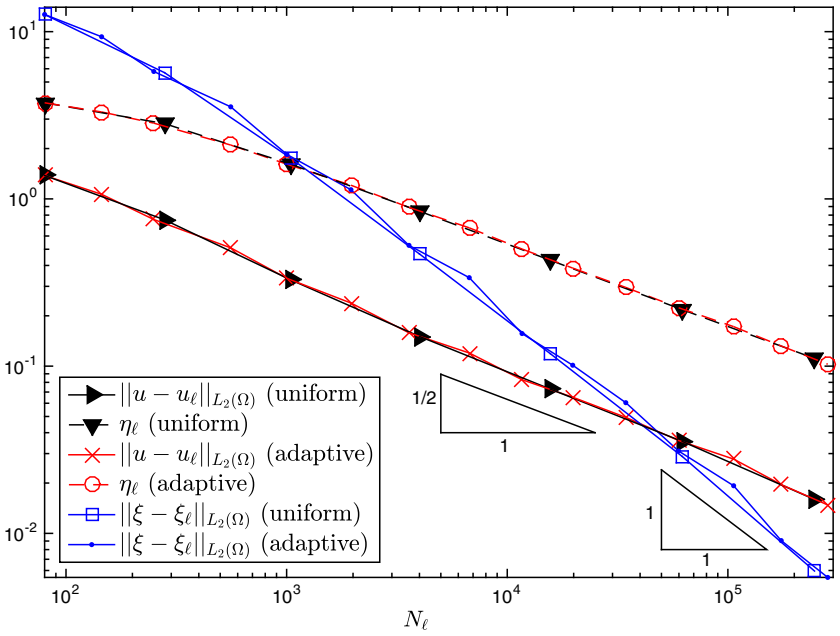

Fig. 6 Convergence history for the semiconductor simulation

$k = 10$, $\boldsymbol{f} \equiv \boldsymbol{0}$ and the homogeneous perfectly conducting boundary condition on the inner boundary, and we use an impedance boundary condition on the outer boundary induced by the plane wave solution $\boldsymbol{p}e^{ik\boldsymbol{d}\cdot\boldsymbol{x}}$ with $\boldsymbol{d} = (1, 0)^t$ and $\boldsymbol{p} = (0, 1)^t$. The convergence history for this example is displayed in Fig. 6.

We observe that both uniform and adaptive refinements lead to optimal $\mathcal{O}(N_\ell^{-1/2})$ convergence for $\boldsymbol{u}_\ell$, which is different from the example in Sect. 4.3. The reasons are (i) the usual interface singularity for the Laplace operator [13] does not occur along the interface between the semiconductor and the vacuum, and (ii) the loss of energy inside the region occupied by the semiconductor (cf. Fig. 7) weakens the effects of the singularities at the reentrant corners of the inner boundary. Note that no reflections are visible in Fig. 7 due to the loss of energy.

As in the previous example $\|\xi - \xi_\ell\|_{L_2(\Omega)}$ and $\|\xi - \xi_\ell\|_{L_2(\Gamma_{\text{imp}})}$ (not shown) are of higher order.

Remark 7 The asymptotic efficiency indices for the first four examples are observed to be between 4 and 6.

4.5 Cloaking Simulation

The fifth example is for a cloaking simulation based on transformation optics [9,16], where a perfectly conducting cylinder is wrapped by a cylindrical cloak of metamaterial. The domain Ω is the part of the square $(-1, 1)^2$ outside the circle centered at the origin with radius $R_1 = 1/4$, where a perfectly conducting boundary condition is imposed. We take μ and ϵ to be 1 outside a larger circle centered at the origin with radius $R_2 = 1/2$. On the annular region $\{x : R_1 < |x| \le R_2\}$, the permeability and permittivity are defined by

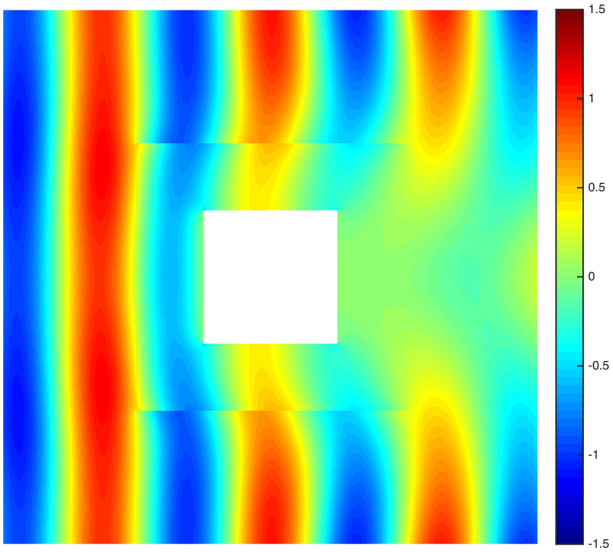

Fig. 7 Real values of the second component of $\boldsymbol{u}_\ell$ for the semiconductor simulation

$$\mu = \left(\left(\frac{R_2 - R_1}{R_2}\right)^2 \frac{r}{r - R_1}\right)^{-1},$$

$$\epsilon_{xx} = \left(\left(\frac{R_2 - R_1}{R_2}\right)^2 + \left(1 + 2\left(\frac{R_2 - R_1}{R_2}\right)^2 \frac{R_1}{r - R_1}\right)\sin^2\theta\right)\mu,$$

$$\epsilon_{xy} = \epsilon_{yx} = -\left(\left(1 + 2\left(\frac{R_2 - R_1}{R_2}\right)^2 \frac{R_1}{r - R_1}\right)\sin\theta\cos\theta\right)\mu,$$

$$\epsilon_{yy} = \left(\left(\frac{R_2 - R_1}{R_2}\right)^2 + \left(1 + 2\left(\frac{R_2 - R_1}{R_2}\right)^2 \frac{R_1}{r - R_1}\right)\cos^2\theta\right)\mu.$$

The right-hand side $\boldsymbol{f}$ for this example is $\mathbf{0}$ and the frequency k is 10. The impedance boundary condition on the outer boundary is induced by the plane wave solution $\boldsymbol{p}e^{ik\boldsymbol{d}\cdot\boldsymbol{x}}$, where $\boldsymbol{d} = (1, 0)^t$ and $\boldsymbol{p} = (0, 1)^t$.

The real part of the second component of the adaptive approximation is shown in Fig. 8. Note that the wave is moving from left to right and that the discrete solution near the right boundary (almost) looks as if the cylinder is not present, i.e., no reflections or shadows are visible. The plot in Fig. 8 is produced with roughly one hundred thousand degrees of freedom, while generating a similar plot with a uniform mesh will require roughly two million degrees of freedom.

An adaptively refined mesh is displayed in Fig. 9 which shows stronger refinement in the region of the cloaking material, especially near the radius $r = R_1$.

Remark 8 Note that the permittivity ϵ is discontinuous at the circle with radius R_2 and it is only positive semi-definite at the circle with radius R_1. Moreover, the permeability μ vanishes at the circle with radius R_1 and hence μ^{-1} does not belong to $L_\infty(\Omega)$. Therefore ϵ and μ do not satisfy the assumptions underlying the a priori analysis in [5] and the *a posteriori*

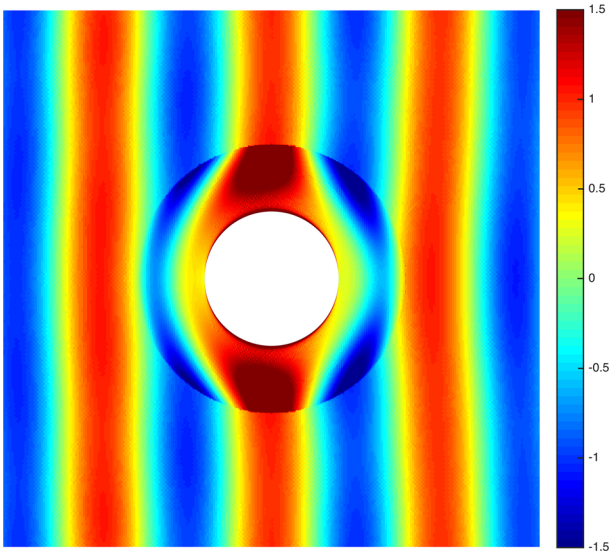

Fig. 8 Real values of the second component of $\boldsymbol{u}_\ell$ for the cloaking simulation

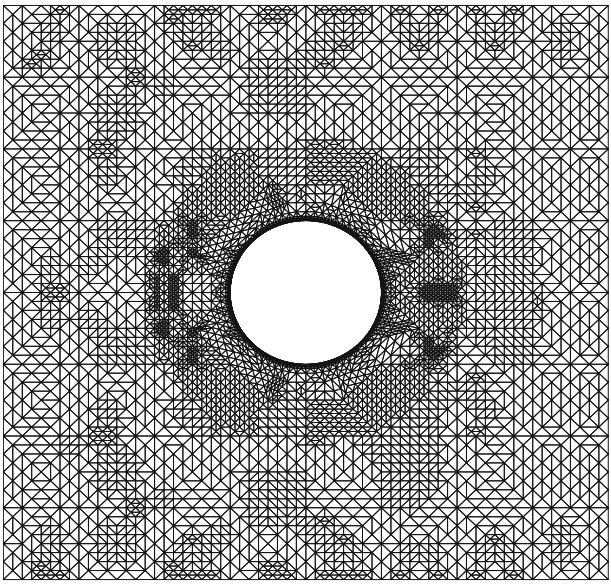

Fig. 9 Adaptive mesh for the cloaking simulation

analysis in Sect. 3. Nevertheless the adaptive P_1 finite element method still works for this example.

4.6 Flat Lens Simulation

For this experiment, Ω is the rectangular domain $(0, 2) \times \left(-\frac{1}{2}, \frac{1}{2}\right)$, $\epsilon = 1$ and $\mu = 1$ outside the rectangle $(7/16, 39/32) \times \left(-\frac{1}{2}, \frac{1}{2}\right)$ and $\epsilon = -1.1$ and $\mu = 1/\epsilon$ inside that rectangle. We

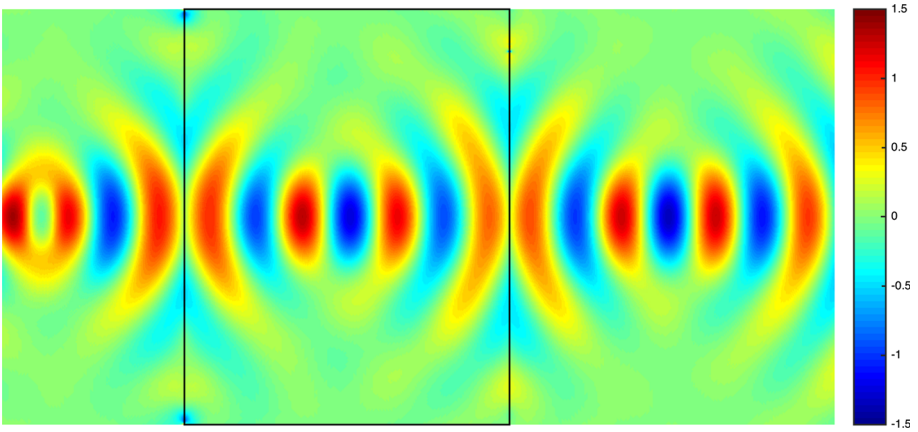

Fig. 10 Real values of the second component of $\boldsymbol{u}_\ell$ for the flat lens simulation. The rectangle with the negative index metamaterial is indicated with *black lines*

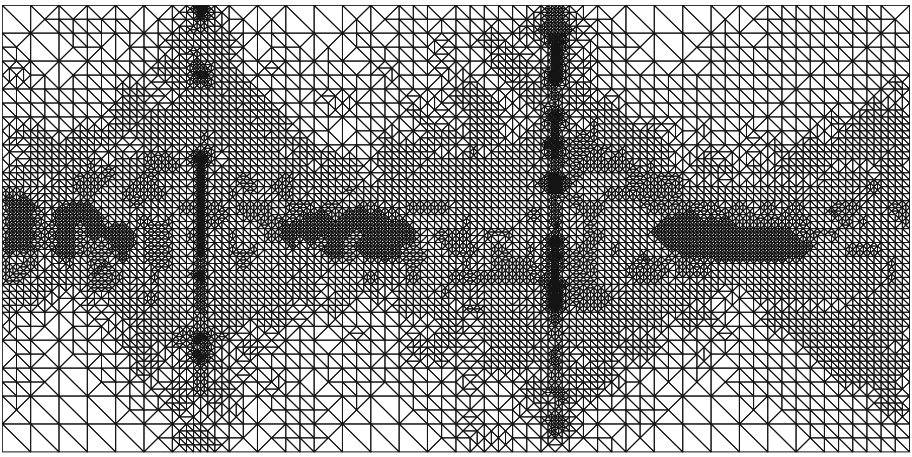

Fig. 11 Adaptive mesh for the flat lens simulation

chose $k = 30$, $\boldsymbol{f} = \boldsymbol{0}$ outside a small square of length $1/16$ close to the left boundary and $\boldsymbol{f} = (0, -2000)^t$ inside that square. The boundary condition is the homogeneous impedance boundary condition.

This example simulates the refocusing effect of a flat lens using a negative index metamaterial with $n = -1$ (cf. [15] and the references therein). The wave emitted from the point near the left boundary of the domain travels from left to right. Once the wave encounters a metamaterial interface it is refocused towards a point as displayed in Fig. 10. The results are similar to those obtained by time domain flat lens simulations [8,20].

Figure 11 shows an adaptively refined mesh. Note that the mesh is more refined at the two vertical interfaces of the metamaterial.

Remark 9 According to the theory in [5, Section 5], the model problem (1) on a simply connected domain with the impedance boundary condition and sign-changing μ and ϵ is a

Fredholm problem if the following condition is satisfied: Given any $w \in H_0^1(\Omega)$ there exists $\zeta_w \in H_0^1(\Omega)$ such that

$$(\epsilon \nabla \zeta_w, \nabla v) = (\nabla w, \nabla v) \qquad \forall\, v \in H_0^1(\Omega).$$

For the flat lens problem considered here, this condition can be verified through the theory developed in [1,2,14]. But the well-posedness of the discrete problems on adaptive meshes and the a priori and *a posteriori* analyses remain open. Nevertheless the adaptive P_1 finite element method appears to also work for this example.

5 Concluding Remarks

By extending the Hodge decomposition approach to include the impedance boundary condition (which can act as an absorbing boundary condition), we are able to solve problems involving the propagation of electromagnetic waves in the frequency domain by solving simple scalar problems with the P_1 finite element.

We have developed a reliable residual based error estimator for the P_1 finite element method and demonstrated numerically that it is also efficient. The resulting adaptive algorithm exhibits optimal convergence in numerical experiments involving general material properties, general domains and general boundary conditions. Proving mathematically the local efficiency of the error estimator is an interesting open problem.

Furthermore we have demonstrated the robustness of the adaptive P_1 finite element method by applying it successfully to a semiconductor problem, a cloaking problem and a flat lens problem whose settings are outside our theoretical framework.

References

1. Bonnet-Ben Dhia, A.-S., Chesnel, L., Ciarlet Jr, P.: T-coercivity for scalar interface problems between dielectrics and metamaterials. ESAIM Math. Model. Numer. Anal **46**, 1363–1387 (2012)
2. Bonnet-Ben Dhia, A.S., Ciarlet Jr, P., Zwölf, C.M.: Time harmonic wave diffraction problems in materials with sign-shifting coefficients. J. Comput. Appl. Math **234**, 1912–1919 (2010)
3. Brenner, S.C., Cui, J., Nan, Z., Sung, L.-Y.: Hodge decomposition for divergence-free vector fields and two-dimensional Maxwell's equations. Math. Comput. **81**, 643–659 (2012)
4. Brenner, S.C., Gedicke, J., Sung, L.-Y.: An adaptive P_1 finite element method for two-dimensional Maxwell's equations. J. Sci. Comput. **55**, 738–754 (2013)
5. Brenner, S.C., Gedicke, J., Sung, L.-Y.: Hodge decomposition for two-dimensional time harmonic Maxwell's equations: impedance boundary condition. Math. Methods Appl. Sci. (2015). doi:10.1002/mma.3398
6. Cui, J.: Multigrid methods for two-dimensional Maxwell's equations on graded meshes. J. Comput. Appl. Math. **255**, 231–247 (2014)
7. Dörfler, W.: A convergent adaptive algorithm for Poisson's equation. SIAM J. Numer. Anal. **33**, 1106–1124 (1996)
8. Li, J., Chen, Y., Elander, V.: Mathematical and numerical study of wave propagation in negative-index materials. Comput. Methods Appl. Mech. Eng. **197**, 3976–3987 (2008)
9. Li, J., Huang, Y., Yang, W.: An adaptive edge finite element method for electromagnetic cloaking simulation. J. Comput. Phys. **249**, 216–232 (2013)
10. Mekchay, K., Nochetto, R.H.: Convergence of adaptive finite element methods for general second order linear elliptic PDEs. SIAM J. Numer. Anal. **43**, 1803–1827 (2005)
11. Monk, P.: Finite Element Methods for Maxwell's Equations. Oxford University Press, New York (2003)
12. Nader, E., Ziolkowski, R.W.: Metamaterials: Physics and Engineering Exploarations. Wiley, New York (2006)
13. Nicaise, S.: Polygonal interface problems. Verlag Peter D. Lang, Frankfurt am Main (1993)

14. Nicaise, S., Venel, J.: A posteriori error estimates for a finite element approximation of transmission problems with sign changing coefficients. J. Comput. Appl. Math. **235**, 4272–4282 (2011)
15. Pendry, J.B.: Negative refraction makes a perfect lens. Phys. Rev. Lett. **85**, 3966–3969 (2000)
16. Pendry, J.B., Schurig, D., Smith, D.R.: Controlling electromagnetic fields. Science **312**, 1780–1782 (2006)
17. Scott, L.R., Zhang, S.: Finite element interpolation of nonsmooth functions satisfying boundary conditions. Math. Comput. **54**, 483–493 (1990)
18. Senior, T.B.A., Volakis, J.L.: Approximate Boundary Condition in Electromagnetics. IEEE Press, New York (1995)
19. Solymar, L., Shamonina, E.: Waves in Metamaterials. Oxford University Press, Oxford (2009)
20. Ziolkowski, R.W.: Pulsed and cw gaussian beam interactions with double negative metamaterial slabs. Opt. Express **11**, 662–681 (2003)